Instabilities and routes to chaos in passive all-optical resonators containing a molecular gas

W. J. Firth, R. G. Harrison, and I. A. Al-Saidi
Department of Physics, Heriot-Watt University, Riccarton, Edinburgh EH14 4AS, United Kingdom
(Received 12 June 1985)

Dispersive optical bistability and instabilities leading to period doubling, higher harmonics, and chaos in an all-optical passive quantum system are discussed theoretically and experimentally. These phenomena have been observed for a wide range of operating conditions in ring and Fabry-Perot resonators containing ammonia molecular gas as the nonlinear medium. Laser input intensity, gas pressure, and cavity tuning are the main control parameters in observation of these effects. The experimental results are well modeled by our generalization of standard two-level system theory to include standing-wave, reservoir, and transverse effects.

I. INTRODUCTION

Nonlinear optical resonators display a wide range of phenomena of fundamental interest. In passive resonators, optical bistability[1] (OB) and related phenomena have attracted much attention. We are concerned in this paper with an outgrowth of optical bistability, which has wide interest in its own right, namely, instabilities and chaos in the output of a (passive) nonlinear resonator. This class of phenomena, currently undergoing intense cross-disciplinary investigation,[2] is illustrated in a particularly interesting manner in optics, since simple behavior characteristics of low-dimensional systems can be obtained,[1,3] while there is the interesting possibility of a quantum description of the phenomena, particularly when the nonlinearity arises from the saturation of two-level atoms.[4]

Ikeda first described an instability with period $2t_R$, where t_R is the cavity round-trip time, in a ring resonator containing a two-level medium,[4] with a period-doubling cascade leading to chaotic output with a continuous wave input.[3] Since then, similar phenomena, including all the "universal" routes to chaos, have been predicted in a wide class of passive optical systems with feedback.[1] Experimental evidence, however, was slow in arriving, and remains patchy. The first demonstration was in a hybrid system with electronic feedback,[5] which provided an enormous stimulus despite its only quasioptical nature. Only in 1984 did the first all-optical demonstration of the Ikeda instability appear in the literature,[6] employing glass fiber as both waveguide and nonlinear medium.

The main reason for the Ikeda instability being much harder to observe than optical bistability itself is the requirement that the response time of the nonlinear medium, τ, be short enough to allow $2t_R$ oscillation, i.e., a "good," or at least fairly good, cavity is required, in order that the medium bandwidth is able to cover two or more adjacent longitudinal cavity modes. There is no such requirement for bistability, e.g., $\tau \geq 10^4 t_R$ is typical for InSb,[7] in which bistability is observable at very low powers because of the resonant nature of the nonlinearity. A nonresonant nonlinearity, on the other hand, will be fast enough for the Ikeda instability, but will require high powers, and there will be no discrimination against competing nonlinear processes—both problems in the fiber experiment,[6] where picosecond pulse excitation was necessary to avoid stimulated Brillouin scattering.

Ideally then, one seeks a medium with a nonlinearity resonantly enhanced sufficiently to outweigh competing processes and reduce power requirements, but with a response time of a few nanoseconds to allow compact resonator design.

Considerations such as these point to gases as optimal media, and we were led to look at molecular gases where there are many absorption lines near to resonance with CO_2 laser lines, while the response time is readily adjustable by pressure variation to obtain the best resonance—response-time trade-off. In particular, ammonia has well-documented coincidences with CO_2 laser lines,[8] and energy levels sufficiently widely spaced to approximate reasonably closely to an ideal two-level system. We recently reported $2t_R$ oscillation in a ring resonator containing NH_3 gas,[9] and subsequently observed bifurcations and chaos in a compact Fabry-Perot resonator, again containing ammonia.[10]

The purpose of this paper is to collate and expand our theoretical models and experimental observations of OB and instabilities leading to chaos in ring and Fabry-Perot optical resonators. We first review in Sec. II the theoretical picture for the OB and instabilities in ring and Fabry-Perot resonators. In Sec. III we describe the nonlinear absorption characteristics of ammonia and molecular energy-level schemes. We then describe in Sec. IV the experimental arrangement and experimental results in comparison with the theoretical predictions. Finally, in Sec. V, we summarize our experimental and theoretical results and discuss possible future developments.

II. THEORY OF INSTABILITIES IN PASSIVE NONLINEAR RESONATORS

In this section we develop and explore the theory of dynamical instabilities and chaos in passive nonlinear resonators in both ring and Fabry-Perot configurations. We discuss the physical basis of the instabilities on the

one hand, and development of models adequate to describe the experimental results presented later, on the other.

Fabry-Perot resonators give effects qualitatively similar to those in ring resonators, but are more complicated to analyze (though simpler and better for experiments). Our first work in this field[11] established the existence of instabilities in Fabry-Perot resonators containing a Kerr medium of zero response time. We subsequently elaborated this model to include finite response times, in the course of which we were able to extract an accurate Feigenbaum cascade,[12] and this led to the present analysis of saturable media, spurred by the successful experiments described below. We will only occasionally consider the role of transverse effects in these phenomena; the reader is referred to Ref. 13 for a much fuller discussion of transverse effects, in ring resonators containing saturable media.

A. The basic model (Ref. 14)

Let us assume that we have a system of two-level atoms of transition frequency ω_0 and dipole moment μ irradiated by a field of frequency ω. Using the density-matrix formalism and splitting the field and polarization into their positive and negative frequency parts,

$$E=E^{+}\exp(-i\omega t)+E^{-}\exp(i\omega t)\ ,$$
$$P=N_a\mu[P^{+}\exp(-i\omega t)+P^{-}\exp(i\omega t)]\ , \tag{2.1}$$

with $E^{+}=E^{-*}$, $P^{+}=P^{-*}$, and N_a the number density of atoms, we obtain in the rotating-wave approximation, and assuming homogeneous broadening,

$$\frac{\partial P^{\pm}}{\partial t}=\left[\pm i\Delta-\frac{1}{T_2}\right]P^{\pm}\mp i\frac{\mu}{\hbar}E^{\pm}n\ , \tag{2.2}$$

$$\frac{\partial n}{\partial t}=-\frac{n+1}{T_1}-2i\frac{\mu}{\hbar}(E^{-}P^{+}-E^{+}P^{-})\ , \tag{2.3}$$

where n is the population inversion, T_1 is the longitudinal relaxation time, T_2 is the transverse relaxation time, and $\Delta=\omega-\omega_0$. Equations (2.2) and (2.3) used in conjunction with Maxwell's wave equation (in the plane-wave approximation)

$$\frac{\partial^2 E}{\partial x^2}-\frac{1}{c^2}\frac{\partial^2 E}{\partial t^2}=\frac{1}{\epsilon_0 c^2}\frac{\partial^2 P}{\partial t^2} \tag{2.4}$$

in the slowly varying envelope approximation constitute the Maxwell-Bloch equations. In the limit $T_2\ll T_1$ we can eliminate $P^{\pm}$ adiabatically (i.e., $\partial P^{\pm}/\partial t\simeq 0$) from Eq. (2.2), so that

$$P^{\pm}=\mp i\frac{\mu T_2}{\hbar}E^{\pm}n\frac{1\pm i\tilde{\Delta}}{1+\tilde{\Delta}^2}\ , \tag{2.5}$$

where $\tilde{\Delta}=\Delta T_2$; substituting Eq. (2.5) in (2.3) and defining the "intensity" $I=E^{+}E^{-}$, we obtain

$$T_1\frac{\partial n}{\partial t}=-(n+1)+n\frac{I}{I_s}\ , \tag{2.6}$$

where I_s is the saturation intensity, given by

$$I_s=\frac{\hbar^2}{4\mu^2}\frac{1+\tilde{\Delta}^2}{T_1T_2}\ .$$

Substituting (2.5) into (2.4) gives, for the positive-frequency component,

$$\frac{\partial^2}{\partial x^2}[E^{+}\exp(-i\omega t)]-\frac{n_b^2}{c^2}\frac{\partial^2}{\partial t^2}[E^{+}\exp(-i\omega t)]$$
$$=\frac{-\omega^2}{\epsilon_0 c^2}\frac{N_a\mu^2T_2}{\hbar(1+\tilde{\Delta}^2)}n(\tilde{\Delta}-i)[E^{+}\exp(-i\omega t)]\ , \tag{2.7}$$

where n_b is the background refractive index of the medium. In the case where the sample is in a Fabry-Perot cavity, E^{+} can be expressed as a sum of forward and backward fields with envelopes $E_F(x,t)$ and $E_B(x,t)$, respectively:

$$E^{+}(x,t)=E_F(x,t)\exp(in_bk_0x)$$
$$+E_B(x,t)\exp(-in_bk_0x),\quad k_0=\omega/c\ . \tag{2.8}$$

Upon substituting Eq. (2.8) in (2.7), and making the slowly varying envelope approximation, we obtain

$$\exp(ikx)\left[\frac{\partial E_F}{\partial x}+\frac{n_b}{c}\frac{\partial E_F}{\partial t}\right]$$
$$+\exp(-ikx)\left[-\frac{\partial E_B}{\partial x}+\frac{n_b}{c}\frac{\partial E_B}{\partial t}\right]$$
$$=+\frac{\alpha_0}{2}\left[\frac{1+i\tilde{\Delta}}{1+\tilde{\Delta}^2}\right]nE^{+}(x,t),\quad k=n_bk_0 \tag{2.9}$$

where $\alpha_0=\omega N_a\mu^2T_2/\epsilon_0n_bc\hbar$ is the on-resonance absorption coefficient.

For bidirectional propagation, n will be a rapidly varying function of z, due to the spatial modulation of I in (2.6). In order to obtain true slowly varying amplitude equations for the evolution of E_F and E_B, it is then necessary to solve (2.6), so as to find the Fourier components of the right-hand side of (2.9) which are phase matched to one or the other of the terms on the left. Before involving ourselves in such complexities, let us first consider ring cavities, and thus set $E_B\equiv 0$ in (2.9). Let us then define, for a medium length L,

$$D(t)=-\frac{1}{L}\int_0^L dx\, n\left[x,t+\frac{n_bx}{c}\right]\ , \tag{2.10}$$

which means that $D(t)$ is (minus) the inversion averaged along the light cone starting from $x=0$ at time t. Some manipulation[4] then enables (2.6) to be written in averaged form as

$$T_1\dot{D}(t)=[1-D(t)]-|\epsilon(t)|^2\frac{1-e^{-\alpha LD(t)}}{\alpha L}\ , \tag{2.11}$$

where $\epsilon(t)=E_F(0,t)/I_s^{1/2}$ and $\alpha=\alpha_0/(1+\tilde{\Delta}^2)$. This ansatz for the population enables an explicit integration of (2.9) along the light cone; the ring-cavity boundary conditions can then be applied to obtain the following relation between ϵ at times separated by one cavity round-trip time t_R:[10]

$$\epsilon(t)=\epsilon_i(t)+R\epsilon(t-t_R)e^{i\theta}\exp\left[-\frac{\alpha L}{2}(1-i\tilde{\Delta})D(t-t_R)\right]. \tag{2.12}$$

Here, $\epsilon_i(t)$ is the scaled incident field (transmitted into the cavity), R is the round-trip amplitude loss (by transmission and any absorption outside the nonlinear medium), and θ is the cavity tuning in the absence of the medium ($\alpha\rightarrow 0$). In the latter case, we see that constant input field leads to a constant forward field

$$\epsilon=\frac{\epsilon_i}{1-Re^{i\theta}} \tag{2.13}$$

showing the usual resonance behavior as θ is varied, e.g., by fine-tuning a cavity mirror. Equations (2.11) and (2.12), supplemented and slightly modified to account for reservoir effects, will be used to analyze experiments on ammonia gas in the following sections.

The effect of the nonlinear medium on the resonator response is best approached by considering first the *dispersive limit* $\alpha L \ll 1$, $|\tilde{\Delta}| \gg 1$, $I \ll I_s$, $I|\tilde{\Delta}| \sim I_s$. If we also assume $T_1 \ll t_R$, then (2.11) gives, approximately,

$$D(t)\approx\frac{1}{1+|\epsilon(t)|^2}\approx 1-|\epsilon(t)|^2$$

so that (2.12) becomes

$$\epsilon(t)=\epsilon_i(t)+R\epsilon(t-t_R)e^{i\theta'}e^{iG|\epsilon(t-t_R)|^2}, \tag{2.14}$$

where $G=\alpha L\tilde{\Delta}/2$, and θ' includes the linear phase shift due to the gas. In this limit, the original system of differential equations and boundary conditions is reduced to a nonlinear *mapping* of the cavity field at intervals of t_R, the round-trip time, as first obtained by Ikeda.[4] He showed that the fixed points of (2.14) are, in general, multiple-valued functions of the input field, giving optical multistability, More significant here, however, was his demonstration that the Ikeda map can show period-doubling cascades leading to chaos, in which $\epsilon(t)$ wanders on a *strange attractor* (of fractional dimension) in its complex phase plane.

B. Physical interpretation of the Ikeda instability

The material nonlinearity responsible for nonlinear refraction, and thus bistability, can also generate sidebands on the pump frequency. Physically, two photons with frequency ω are scattered to form a pair of photons at $\omega\pm\Delta\omega$, so the process is termed four-wave mixing. An additional input signal, the probe, detuned from the pump by $\Delta\omega$ will thus experience gain or loss according to the combined effect of the nonlinearity and the mode structure of the cavity. Clearly, it is most advantageous if *both* $\omega+\Delta\omega$ and $\omega-\Delta\omega$ are cavity resonant, i.e., if $2\Delta\omega$ is a multiple of the cavity's free spectral range. An *even* multiple (including zero) means that the pump is itself resonant, and this double resonance lies behind optical bistability and the sideband instabilities analyzed by Lugiato and co-workers.[15] An odd multiple, on the other hand, means that the pump is off resonance, lying exactly halfway between two modes: the beat note between the pump and the resonant sidebands (which will be self-excited if the nonlinearity is strong enough) then has period $2t_R$, identifying this as the Ikeda instability.

The nice thing about this system is that the preceding double resonance can be guaranteed: the refractive-index change induced by the strong pump beam actually moves the comb of longitudinal modes with respect to the pump frequency, and this "transphasing" of the mode spectrum alternately gives rise to bistable and Ikeda-type double resonances as the pump parameter ϵ_i is increased.[16] This is illustrated in Fig. 1.

The entire period-doubling cascade can be given a similar interpretation. As each new period $2^n t_R$ bursts into oscillation the effective free spectral range of the cavity is halved because the generalized condition for resonance must be constructive interference after 2^n trips (since only after $2^n t_R$ do the cavity's optical properties repeat themselves). At the $2^n t_R$ threshold these small-signal modes are degenerate with the oscillating frequency spectrum, but as ϵ_i is increased, they "transphase" in frequency to halfway between the oscillating frequencies. If the gain there becomes large enough, these new modes burst into oscillation; if not, "transphasing" continues (Fig. 1) to a renewed coincidence with the oscillating frequencies, at which point an inverse period-doubling cascade ensues, leading eventually to a steady-state response. Figure 2 illustrates this process, showing the small-signal gain spectrum as ϵ_i is increased through the $2t_R$ threshold, and the ensuing doubling of the spectrum followed by "transphas-

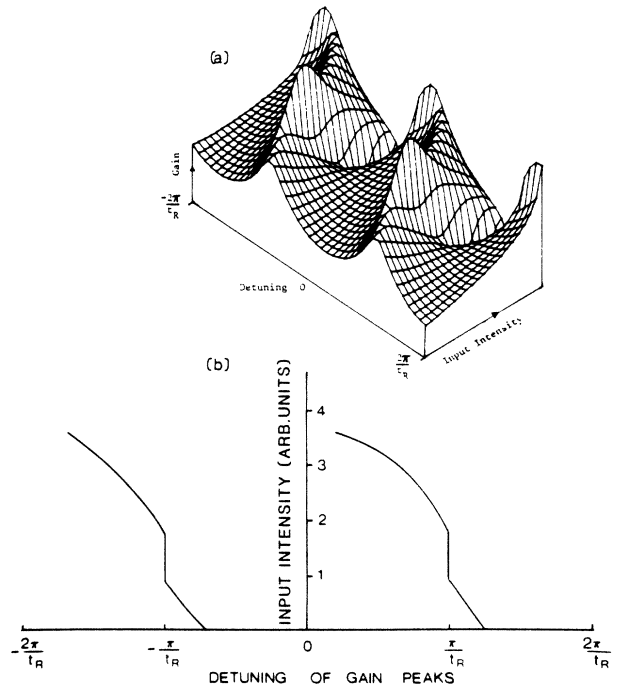

FIG. 1. Gain spectrum for a ring resonator, $B=0.58$, $\theta_0=2.3$, showing "transphasing" of the cavity resonances as the input intensity is increased, together with locking at the Ikeda $2t_R$ resonance position (B is the amplitude feedback factor of the cavity, and θ_0 the mistuning).

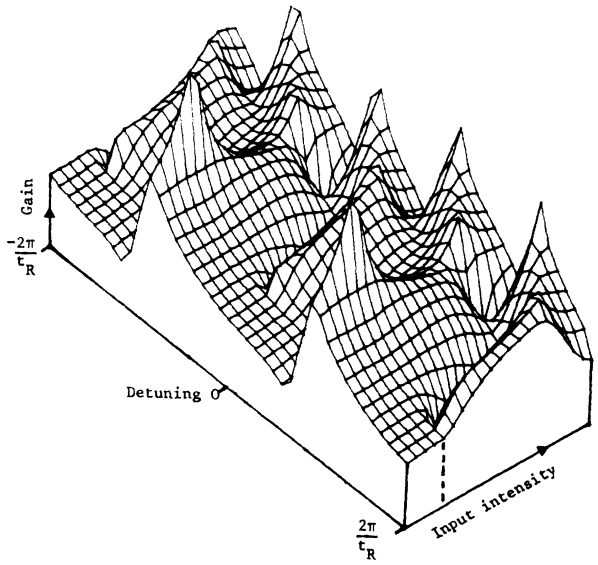

FIG. 2. Gain spectrum for a ring resonator showing the creation of new "modes" at a bifurcation (steady state $\rightarrow 2t_R$ oscillation). The bifurcation point is marked by the dotted line. The four peaks at the back indicate the approach to the $2t_R \rightarrow 4t_R$ bifurcation.

ing" to the verge of $4t_R$ oscillation. It should be noted that the noise spectrum of the system should be very similar to Fig. 2, because of the filtering action of the cavity on any broadband noise source.

Considering now finite T_1, perturbation theory readily leads to the conclusion that the gain spectrum of four-wave mixing becomes Lorentzian, with half-width $\sim T_1^{-1}$, and the associated dispersion means that the free spectral range becomes a function of frequency. The former is usually the more important: clearly if $t_R \ll T_1$ then there will be no significant gain in the Ikeda situation, where the modes straddle the pump frequency; this is the physical origin of the requirement $t_R > T_1$ usually quoted for Ikeda instability.

Another effect of finite T_1 is to raise the degeneracy by which all symmetrically placed pairs of sideband modes reach threshold simultaneously. On the one hand, the raising of the OB degeneracy permits self-pulsing at period t_R, as described by Lugiato *et al.*,[15] while on the other, the Ikeda degeneracy splits to yield pulsing at $2t_R/3$, $2t_R/5$, etc. These high-frequency instabilities have been extensively studied in hybrid systems:[17] we have observed the $2t_R/3$ oscillation in an all-optical system based on ammonia gas (see below).

C. Fabry-Perot resonators

We now resume discussion of the case where E_B is nonzero in (2.8), appropriate to Fabry-Perot resonators. For finite T_1, progress can only be made in the dispersive limit, where the spatial modulation of n in (2.6), induced by that implicit in I, is small, so that only Fourier components of low order need be considered. This is not the case, however, for a highly saturated medium, such as we deal with in the experiments described below, so we first take the limit $T_1 \rightarrow 0$ in (2.6), so that

$$n(1+I/I_s)=1 \ . \tag{2.15}$$

Writing

$$I=|E_F|^2+|E_B|^2+E_F E_B^* e^{2ikz}+\text{c.c.}$$
$$=(I_0+G+G^*)I_s \ , \tag{2.16}$$

where G describes the spatial grating in the standing-wave field, we seek to solve (2.15) by the ansatz

$$n=n_0+\sum_{j=1}^{\infty}(n_j G^j+\text{c.c.}) \ ,$$

which, on insertion into (2.15), gives, for the spatially uniform (dc) term,

$$(1+I_0)n_0+|G|^2(n_1+n_1^*)=1 \tag{2.17}$$

and for the term $\sim e^{i2jkz}$,

$$(1+I_0)n_j+n_{j-1}+|G|^2 n_{j+1}=0 \ . \tag{2.18}$$

This equation has solutions in which

$$\frac{n_j}{n_{j+1}}=\frac{-(1+I_0)\pm[(1+I_0)^2-4|G|^2]^{1/2}}{2}$$

$$\text{for all } j>0 \ . \tag{2.19}$$

In order that the degree of spatial modulation decrease with j, the lower sign must be chosen. Furthermore, all n_j are real.

Use of (2.19) in (2.17) enables n_0 to be calculated:

$$n_0=[(1+I_0)^2-4|G|^2]^{1/2} \ , \tag{2.20}$$

which reduces to the previous expression in the case of unidirectionality ($G=0$). n_1 can be obtained from (2.19):

$$n_1/n_0=\frac{-(1+I_0)+[(1+I_0)^2-4|G|^2]^{1/2}}{2|G|^2} \ . \tag{2.21}$$

The terms on the right-hand side of (2.9) phase matched to the forward and backward fields can now be found:

$$\langle nE^+\rangle_F=n_0E_F[1+(n_1/n_0)E_B^2/I_s] \ , \tag{2.22a}$$

and

$$\langle nE^+\rangle=n_0E_B[1+(n_1/n_0)E_F^2/I_s] \ . \tag{2.22b}$$

The population-grating term n_1 thus gives rise to *nonlinear nonreciprocity:* the absorption coefficient and refractive index experienced by the forward-and backward-traveling waves are *unequal.*

For weak fields, we find

$$n_0 \simeq 1-I_0, \quad n_1=-n_0 \ ,$$

and thus we obtain from (2.22),

$$\langle nE^+\rangle_F=E_F[1-(|E_F|^2+2|E_B|^2)/I_s] \ ,$$
$$\langle nE^+\rangle_B=E_B[1-(2|E_F|^2+|E_B|^2)/I_s] \ ,$$

and we see that the mutual nonlinear effect is double the

self-effect.

Instabilities in Fabry-Perot resonators with saturable two-level media, which require the full equations (2.9) and (2.22), have received little, if any, study, but we present below results of computations based on these equations showing period doubling and chaos.

III. NONLINEAR ABSORPTION CHARACTERISTICS OF AMMONIA

Many molecular gases have near-resonant vibrational-rotational (V-R) transitions with the CO_2 laser in the 9—10-μm spectral region providing a range of frequency offsets well documented from photochemistry studies.[18]

Of these, ammonia is selected here as a particularly attractive candidate for investigation since it typifies a discrete level system in which excited-state pumping is in general precluded by significant anharmonicity, inversion splitting, and large rotational constant.[19] As such, several of the V-R transitions of the ν_2 fundamental band act as two-level systems when pumped by CO_2 laser radiation. As fundamentally the simplest of nonlinear schemes, which can be furthermore fully quantized, the two-level medium merits special attention.

Nonlinear refraction in near-resonantly excited media, which is the fundamental mechanism responsible for the instability phenomena considered here, arises from intensity-dependent saturation of anomalous dispersion.

The laser-induced energy transfer processes which give rise to this may be understood from investigation of the accompanying effect of saturated absorption. Using this approach we find our data for NH_3 are well modeled using a simplified energy-level scheme describing the molecule. This theory is subsequently applied to nonlinear optical resonators in the interpretation of the instabilities observed in these systems; viz., both ring and Fabry-Perot cavities containing NH_3 gas.

Since the generation of resonant nonlinearity depends on partial saturation of the optically pumped transition, molecules with low saturation intensity are ideal. However, the counteracting requirement of fast medium response time for generation of instabilities implies high saturation intensities. To meet these conditions for NH_3, and indeed for most polyatomic molecules, we are restricted to saturation effects arising from rotational relaxation rather than from vibrational-translational relaxation, which is relatively slow. Relatively high-power pump signals are therefore required necessitating the use of pulsed rather than cw laser systems.

In our experiments a transversely excited atmospheric (TEA) CO_2 laser operated on a single transverse and longitudinal mode was used, providing step-tunable (step interval ~ 2 cm^{-1}) smooth pulses full width at half maximum (FWHM) ~ 100 ns and peak power ~ 1 MW. Mode control was achieved by injection locking[20] of the TEA laser using the signal from a frequency-stabilized cw CO_2 laser. Alternatively, a cw CO_2 gain section was incorporated within the cavity of the TEA system; the so-called hybrid system.[21]

Ammonia absorption measurements were taken over an extended pressure range using short cell lengths of 10—20 cm to minimize self-focusing effects, so ensuring an essentially constant beam cross section throughout the medium. The TEA CO_2 laser input and transmitted signals were sampled by KBr beam splitters and monitored by photon drag detectors and a Tektronix 7104 oscilloscope, total response time ≤ 1 ns. Typical input and output pulse shapes are shown in Fig. 3 for a fixed input intensity of ~ 3 MW/cm^2. Data here are for the $aR(1,1)$ transition which lies 1.23 GHz below the $10R(14)$ CO_2 laser pump line[22] and is representative of that obtained for other optically pumped transitions. Effects of saturation, clearly evident at low pressure, diminish with increased pressure resulting in a progressively weaker, narrower, and apparently delayed transmitted signal. Additional measurements of small-signal absorption, using a low-power cw CO_2 input signal are shown in Fig. 4. The good pressure-squared dependence of the absorption coefficient

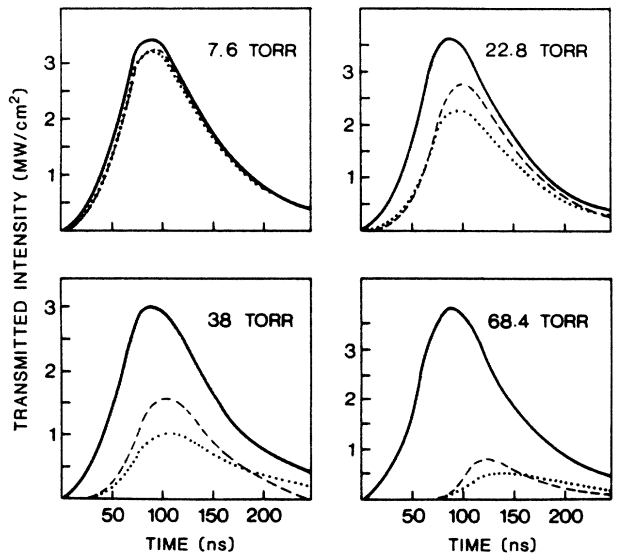

FIG. 3. CO_2 laser pulse transmission through NH_3 for various pressures: input pulse (solid line); transmitted pulse, (a) experimental (dashed lines), (b) computed (dotted lines).

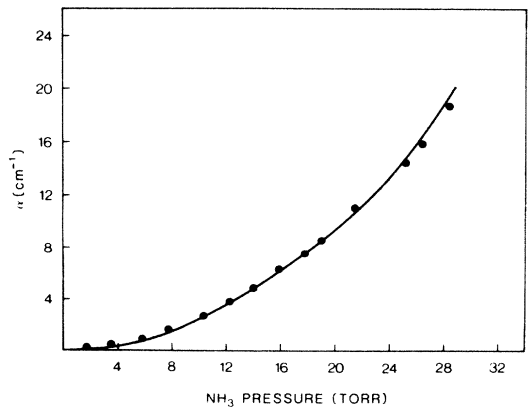

FIG. 4. Small-signal absorption coefficient (α) as a function of the NH_3 pressure: experimental (dotted line); and theoretical (solid line).

confirm that the system acts on an off-resonantly pumped, homogeneously broadened two-level system, yielding a value for α for 0.025 cm^{-1} at 10 Torr.

A. Molecular energy-level scheme

Population redistribution in optically pumped molecular systems is determined by the interplay between such factors as the pump intensity, pump-pulse duration, and the various molecular relaxation processes responsible for redistributing the excited population among the vibrational-rotational energy states of the molecule.

Of these, rotational inelastic collisions involve the smallest energy change [(rotational level spacing) $\sim 10^{-2} \times$ (vibrational level spacing)] and consequently rotational relaxation is usually the fastest of these processes ($\sim 10^{-9}$–10^{-10} atm s). This is, therefore, the dominant pressure-dependent contribution to line broadening. Following excitation of a particular vibrational-rotational transition, population is then rapidly thermalized among the manifold of rotational states of the ground and excited vibrational levels. Subsequent deexcitation of population to ground occurs at a considerably slower rate normally through vibrational-translational (V-T) relaxation (10^{-5}–10^{-8} atm s). We note that, at least for low levels, vibrational-vibrational (V-V) relaxation between like molecules, although often faster than V-T relaxation, does not in general contribute appreciably to population redistribution. Similarly, spontaneous radiative emission, which is extremely slow in the infrared ($\gtrsim 10^{-2}$ s), has little effect.

A typical energy-level scheme showing the relevant levels for the ν_2 fundamental band, of NH_3, is illustrated in Fig. 5(a), showing the radiatively coupled vibrational-rotational (V-R) transition and collisional relaxation routes. For the purpose of analysis it is convenient to represent this scheme in the simplified form shown in Fig. 5(b), where n_1 and n_2 are the number densities of the molecules in the vibrational-rotational level interacting with the CO_2 pump laser and N_1 and N_2 represent the number densities of all other molecules in the states of the same vibrational mode.

The radiative coupling between the pumped transitions is shown by continuous lines, and the corresponding rate coefficients are $W_{lm} = I(t)\sigma_{lm}/\hbar\omega$ (s^{-1}), where σ_{lm} is the absorption cross section, $I(t)$ the pump-laser intensity, and $\hbar\omega$ the pump-photon energy.

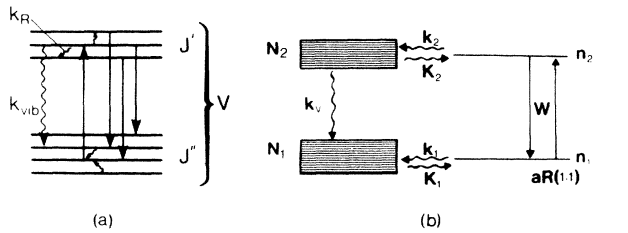

FIG. 5. (a) Energy levels and transitions for pumping and lasing processes. (b) Kinetic model scheme representative of the energy-level scheme in (a). Radiative coupling is represented by continuous lines and collisional relaxation (both rotational and vibrational) by wavy lines.

Collisional relaxations (both rotational and vibrational) are shown by wavy arrows and corresponding rate coefficients linking levels l and m are denoted by k_{lm} ($Torr^{-1}s^{-1}$). Vibrational cross relaxations are omitted for the sake of clarity in illustration.

The genesis of our model can be traced to the work of Burak *et al.*,[23] in which they provided justification for treating the molecular densities N_1 and N_2 as single kinetic groups. The implication of this treatment is that rotational-level populations constituting the kinetic group N_1 (or N_2) relax together, maintaining their thermal equilibrium distribution. It was further shown that the equilibrium rate law between the rotational relaxation rates, namely,

$$k_{lm} = (f_m/f_l)k_{ml} , \tag{3.1}$$

where f_l is the thermal equilibrium fractional population of the level l, can reasonably be extended to the nonequilibrium case of pumping. The equations describing energy transfer are considerably simplified by considering only those collisional relaxation processes that make a dominant contribution to population redistribution among the levels. These are V-V and V-T or V-R relaxation from the manifold of rotational states comprising N_2 to those comprising N_1 (rate constant k_v) and the rotational relaxation of population between the pumped level and these manifolds. Specifying the rotational relaxation rates from levels 1 and 2 as k_1 and k_2, respectively, then the rates from the manifolds to these states, K_1 and K_2, respectively, are determined by detailed balance, Eq. (3.1). The rate equations then can be written as

$$\frac{dn_1}{dt} = -W\left[n_1 - \frac{g_1}{g_2}n_2\right] - k_1 n_1 + K_1 N_1 , \tag{3.2}$$

$$\frac{dn_2}{dt} = W\left[n_1 - \frac{g_1}{g_2}n_2\right] - k_2 n_2 + K_2 N_2 , \tag{3.3}$$

$$\frac{dN_1}{dt} = -K_1 N_1 + k n_1 + k_v N_2 , \tag{3.4}$$

$$\frac{dN_2}{dt} = -K_2 N_2 + k_2 n_2 - k_v N_2 , \tag{3.5}$$

which imply the conservation of population

$$N = n_1 + n_2 + N_1 + N_2 . \tag{3.6}$$

General consideration of these equations is given in Ref. 24. Here we concentrate on the solution specific to our experimental conditions. For simplicity we assume equal level manifold rate constants in the two levels $k_1 = k_2 = k$ and $K_1 = K_2 = K$. The degeneracy factor g_1/g_2 is $\frac{3}{5}$ for the $aR(1,1)$ transition and for our conditions k_v, the V-T rate, is negligibly small.

These equations conserve $(n_1 + n_2) = n_e$ and $(N_1 + N_2) = N_e$ separately (e relating to thermal equilibrium); if k, K cannot be set equal in the two levels, generalization is straightforward. Detailed balance requires that $kn_e = KN_e$; in the infinite reservoir limit K thus goes to zero and the system has effectively just two levels with appropriate dynamics. In NH_3 however, $n_e/N_e \sim 2\%$ and $K \sim 2\ \mu s^{-1} Torr^{-1}$. The major effect of finite K is a

leaching of ground-manifold population on a time scale K^{-1} (which is comparable to our pulse duration at the operational pressures) due to equilibration of population between the ground and excited manifolds.

In applying this model to the absorption data of Fig. 3 and subsequently the nonlinear resonator data, we have to consider pressure scaling and spatial effects. The rates k,K are assumed linear in pressure, and consequently the small-signal absorption coefficient is $\sim p^2$ at low pressure (off-resonance), as confirmed from small-signal absorption measurements (Fig. 4). We adopt a value 13 MHz for the FWHM at 1 Torr,[10] which leads to a value 80 MHz/Torr for k: K is 2.1% of k. These values lead to a saturation intensity of 2.31 MW cm^{-2} at 1 Torr (independent of pressure at low pressure). Provided diffraction is negligible, which is an excellent approximation for the single-pass experiments at least, we can account for both longitudinal and radial variation of the field in the gas cell. The former is achieved by a retarded-time spatial averaging as discussed in Sec. II, giving

$$\dot{D}=k[(g+1)N-g-D-(g+1)|\epsilon(t)|^2(1-e^{-\alpha LD})/2\alpha L], \quad (3.7)$$

$$\dot{N}=K[(D+g)/(1+g)-N], \quad (3.8)$$

where $g=g_1/g_2$, and [compare (2.10)]

$$D(t)=\langle n_1-gn_2\rangle/n_e$$

and $N(t)=\langle N_1\rangle/N_e$, and where $n_{2e}=N_{2e}=0$ is assumed for simplicity.

We integrate these equations by a Runge-Kutta method, using a fit to the observed input pulse shape for $I(0,t)$. Transverse effects are included by using the identity for the transmitted power P_t,

$$P_t(t)=\int_0^\infty 2\pi r\,dr\,I_t(r,t)=\tfrac{1}{2}\pi w^2 I_s\int_0^{I_0/I_s} dI\,e^{-\alpha LD(I,t)}, \quad (3.9)$$

where I equals $|\epsilon(t)|^2$. The transmitted power is thus calculated by summing the transmissions, calculated from Eqs. (3.7)–(3.9), of pulses which all have the same time dependence, but whose peak intensities vary from zero in the wings to I_0 in the center.

Using this model with the above parameter values, the observed pump powers and beam area $\frac{1}{2}\pi w^2=0.35$ cm^2, we compute the dotted pulse shapes in Fig. 3, which represent a very satisfactory fit to experiment with no free parameters, and justify our model.

IV. OPTICAL BISTABILITY AND INSTABILITY GENERATION IN OPTICAL RESONATORS

A. Ring resonator

The original optical scheme described by Ikeda[4] for the generation of oscillation and turbulence was a ring cavity containing a two-level nonlinear medium. In our initial cavity experiments we have therefore considered this scheme comprising a unidirectional ring system containing NH_3 gas.[9] As discussed above, the $aR(1,1)$ transition of NH_3 is off-resonantly pumped at 10.3 μm by pulsed emission from a TEA CO_2 laser. The scheme is illustrated in Fig. 6. The laser pulses are coupled with use of a single-surface Ge flat ($R=36\%$) into a 3.5-m three-element ring cavity closed by 100% gold mirrors, containing the gas cell. The input and cavity signals were sampled by KBr beam splitters, and monitored by photon-drag detectors and a Tektronix model 7104 oscilloscope; total response time was $\lesssim 1$ ns. For NH_3 pressures ~ 9–15 Torr, significant self-focusing was observed in single-pass experiments, confirming a nonlinear refractive-index contribution[25] substantial enough for dispersive optical bistability and Ikeda instability. Closing the ring caused a huge distortion of the pulse shapes (sampled after the NH_3 cell). In particular, a considerable proportion of these showed modulation at the 23.4-ns period expected for Ikeda oscillation in our system.[9] Figures 7(b) and 7(c) show representative examples of this modulation, Fig. 7(a) shows the input pulse shape. To confirm the period, we have digitized and Fourier transformed the traces; the resulting spectra show pronounced peaks at ~ 45 MHz, confirming our observation of Ikeda instability. Subsidiary peaks at $(4t_R)^{-1}$, possibly indicating a further bifurcation, have also been observed for some of the oscillatory signals. In contrast the input pulse, Fig. 7(a) has an essentially featureless spectrum.

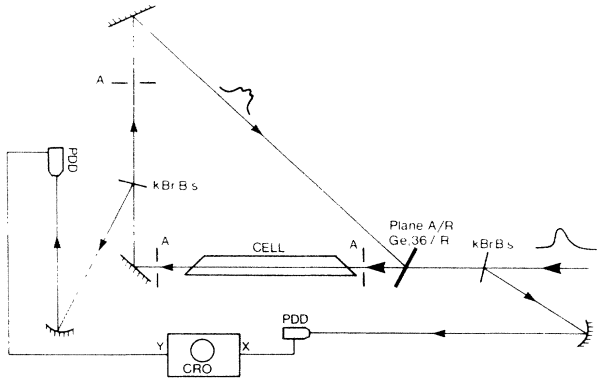

FIG. 6. Schematic diagram of ring-cavity system. B.s., beam splitter; PDD, photon-drag detector; A/R, antireflection coated.

At other cavity settings strong pulse distortion indicative of optical bistability was observed.[26] Examples are shown in Fig. 8(a).

As discussed earlier, our molecular system is not quite a two-level system since allowance must be made for population transfer within the rotational manifolds. Applying the simplified molecular-energy-level scheme, developed earlier, which accounts for this, to the ring-cavity system we obtain a considerable generalization of Ikeda's model. The same assumptions previously used in modeling the nonlinear absorption data are used here.

We have numerically integrated Eqs. (3.7) and (3.8) together with (2.12) using the pump pulse of Fig. 7(a) as input, and Fig. 8(b) shows the predicted intracavity pulses as a function of cavity tuning for representative parameter

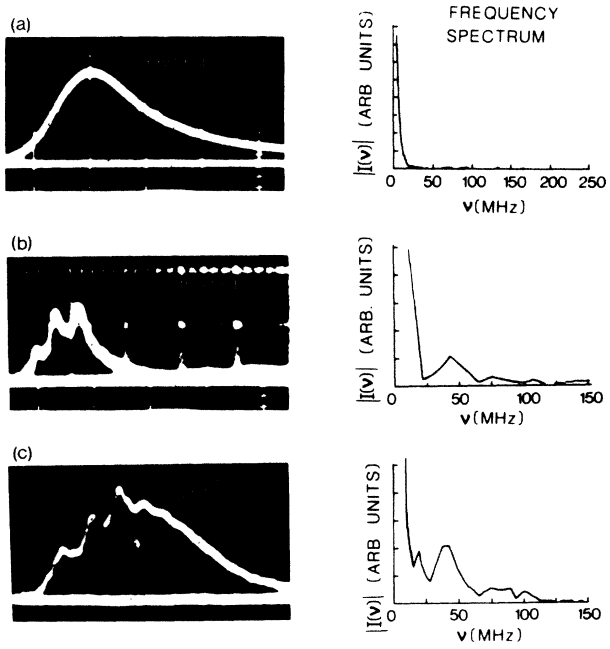

FIG. 7. Sample oscilloscope traces of (a) the pump signal, and (b) and (c) the ring-cavity signal, together with their frequency spectra showing period $2t_R$ in (b) and (c) with indication of $4t_R$ in (c).

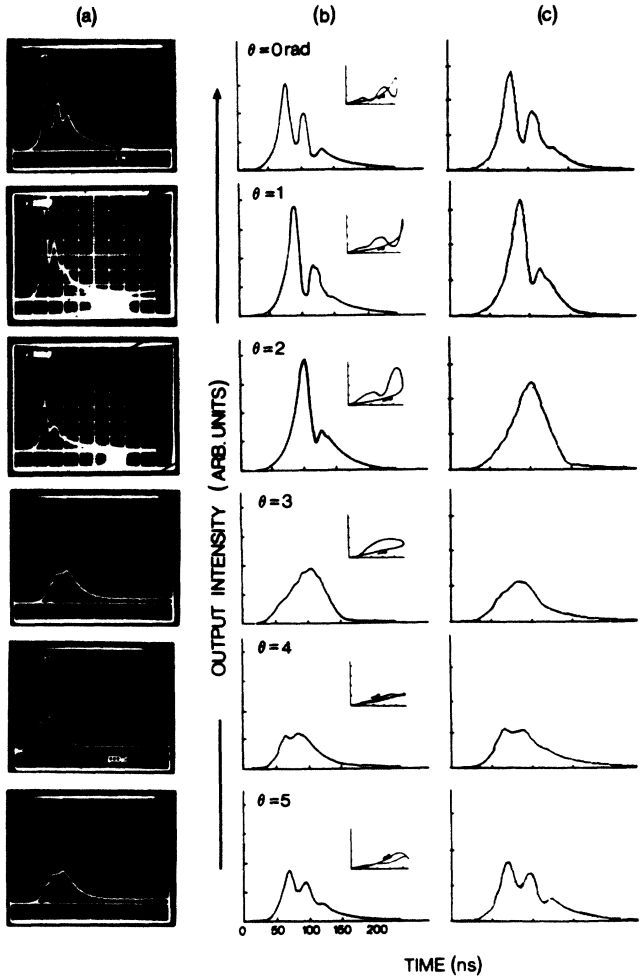

FIG. 8. Sample oscilloscope traces: (a) the ring-cavity signal, together with corresponding theoretical pulse shapes for various detuning angles θ; for (b) the four-level scheme (also showing hysteresis curves of instantaneous cavity signal intensity against incident signal intensity) and (c) the two-level scheme. ($\alpha L=3$, $kt_R=5$, $Kt_R=0.1$, $|\epsilon|^2_{\max}=0.9$.)

values. For comparison of our model with a pure two-level scheme we also show in this figure [8(c)] corresponding traces with K set equal to zero. Results are seen to be in good agreement. Considering data for our generaized four-level scheme [Fig. 8(b)] oscillation at $2t_R$, to be compared with traces of Fig. 8(c), is manifest in the top and bottom traces, which are for similar cavity detuning of $\theta=0$ and 5 rad, while strong pulse distortion, associated with optical hysteresis [see inserts of instantaneous input (x axis) versus output (y axis) signal] occur at the opposite tuning as expected (see Sec. II). In view of the fact that our present model neglects self-focusing, this range of behavior matches extremely well the pulse shapes we observed [Fig. 8(a)].

B. Fabry-Perot resonator

Compared to the ring cavity the Fabry-Perot resonator is a compact and versatile system particularly amenable to parametric studies of instability effects. Admittedly, interpretation of these phenomena is complicated by the effects of standing waves as discussed earlier. The macroscopic behavior of the system is nevertheless expected to be similar to that for the ring system.

To provide a basis for comparison with our data for the ring cavity we again concentrate on the $aR(1,1)$ NH_3 transition pumped by the 10.3-μm pulsed output from a single-mode TEA CO_2 laser. Fabry-Perot resonators of various lengths 20—150 cm with intracavity NH_3 cells of 5—40 Torr were investigated (Fig. 9).

A 17-m optical-delay line prevented significant feedback from the nonlinear resonator to the laser. The Fabry-Perot resonator comprised in most investigations a single-surface Ge flat input coupler of reflectivity $R_0=36$—85% and a single-surface Ge output coupler, of 2-m radius of curvature and reflectivity $R_L=76\%$. The intracavity NH_3 gas cells, of length 10—100 cm, were terminated with KBr Brewster windows. As in the ring experiment, the input signal, sampled by a KBr beam split-

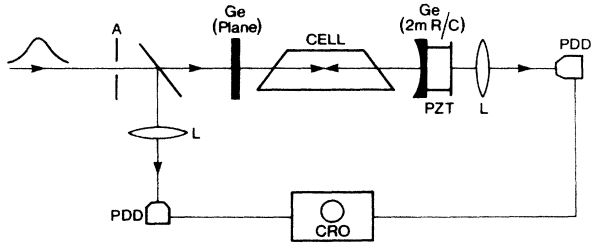

FIG. 9. Schematic diagram of Fabry-Perot cavity system.

ter, and the output signal were monitored by photon-drag detectors and a Tektronix model 7104 oscilloscope. The output coupler was equipped with piezoelectric (PZT) tuning encompassing one free-spectral range of the Fabry-Perot resonator; for an empty cavity the temporal profile of the transmitted signal was identical with that of the input, and showed the expected variation in signal strength with PZT tuning, Fig. 10(a). The transverse intensity profile of the input signal was spatially monitored using conventional pinhole-sampling techniques and shown to be Gaussian with a $1/e$ spot diameter of ~ 3 mm.

The effects obtained with NH_3 were huge; the transmitted signal showed large pulse distortion and modulation, the structure of which was sensitive to NH_3 gas pressure, cavity tuning, and input-signal intensity. Of the various gas cells investigated optimum performance was obtained for lengths of 50—70 cm; optimum gas pressure decreased approximately linearly with increased cell length. The modulation period of the transmitted signal scaled linearly with cavity length, as expected.

Representative examples of the modulated output for PZT tuning are shown in Fig. 10(b) for cavity length 86 cm, cell length 70 cm, and pressure 10 Torr with input coupler reflectivity 67%. Strong Ikeda oscillation (period ≈ 13 ns, fairly close to $2t_R = 11.5$ ns), persistent throughout the pulse, is evident in the neighborhood of minimum transmission, consistent with the four-wave mixing interpretation of this instability discussed earlier. (Note that in contrast to the ring resonator the Fabry-Perot geometry does not prescribe $2t_R$ as the basic period for Ikeda oscillation.) PZT tuning of the cavity leads progressively to "switching" behavior with high peak transmission followed by damped oscillation of longer period. At lower pressures (4—8 Torr), where inhomogeneous broadening may be important, we also obtained strong and sustained $4t_R$ oscillation. A typical PZT scan showing these oscillations in the region of low transmission in shown in Fig. 11(a). At higher pressures (20—30 Torr) much more complex pulse shapes were obtained. These features were enhanced for reduced input coupler reflectivity ($R_0 \simeq 36\%$), since large input coupling is needed to bleach the high absorption ($\alpha L = 6$) to achieve adequate cavity feedback. The PZT sequence shown in Fig. 11(b) for a pressure of 19 Torr shows $2t_R$ oscillation (top trace), developing to $2/3t_R$ oscillation on the higher branch, bifurcating to $4/3t_R$ before again evolving to lower-branch $2t_R$ modulation (bottom trace). Aperiodic pulse shapes, characteristic of chaos, are also evident here and in other data taken at similar pressures. An example for ammonia pressure 15 Torr is shown in Fig. 11(c) where aperiodic pulse shaping is clearly evident in the middle traces. We have undertaken spectral analysis of these pulse shapes, and find strong sharp lines for the oscillatory traces; the aperiodic traces give a broad spectrum with weak structure, as expected for chaos, though pulsed operation perforce reduces the utility of spectral evidence in the identification of chaos.

Our modeling of this system is based on the standing-wave analysis Sec. II for a fully saturable medium,[10] but in the limit $T_1 \to 0$ necessary for the validity of the analysis. This is probably quite a good approximation at NH_3 pressures above 10 Torr, and at lower pressure inhomogeneous broadening ought to be considered in any case. The field equations, using (2.9) and (2.22), become

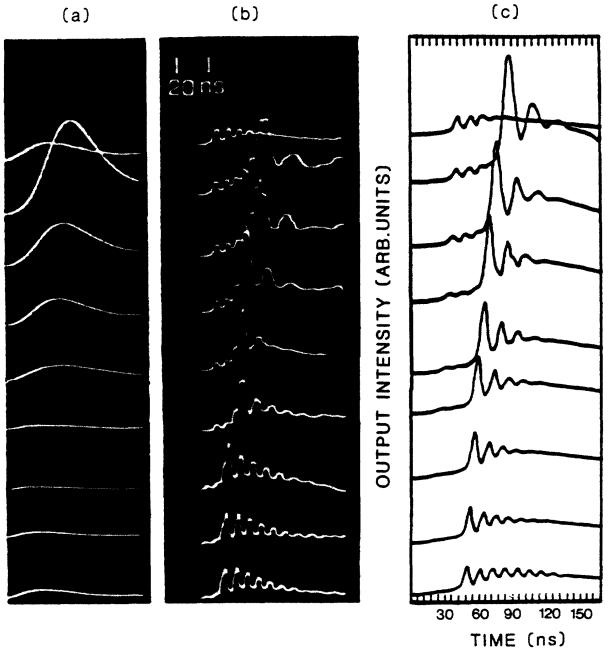

FIG. 10. PZT scan of (a) empty cavity; (b) cavity with 10 Torr NH_3 in 70-cm cell ($L = 86$ cm); input and output reflectivities 67% and 76%, respectively; (c) computer traces for parameters corresponding to (b); $\alpha L = 1.5$, $\Delta \sim 10$; tick spacing t_R.

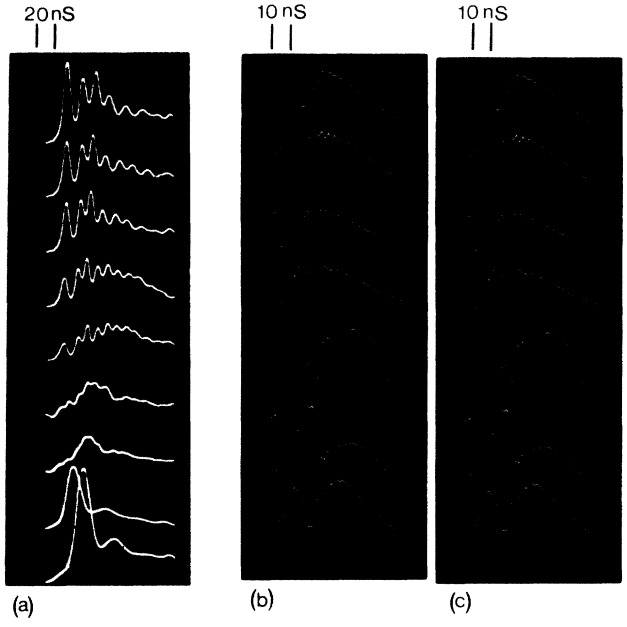

FIG. 11. PZT scan showing (a) $4t_R$ modulation at 5.5 Torr; (b) $2t_R$, $2t_R/3$, and $4t_R/3$ modulation at 19 Torr; and (c) aperiodicity in the modulation at 15 Torr. Cavity parameters as for Fig. 10 but with $R_0 = 36\%$.

$$\frac{\partial E_F}{\partial x}+\frac{n_b}{c}\frac{\partial E_F}{\partial t}=\frac{\alpha_0}{2}\left[\frac{1+i\tilde{\Delta}}{1+\tilde{\Delta}^2}\right]n_0\left[1+\frac{n_1}{n_0}\frac{|E_F|^2}{I_s}\right]E_F$$

$$=f(|E_F|^2,|E_B|^2)E_F \tag{4.1}$$

$$-\frac{\partial F_B}{\partial x}+\frac{n_b}{c}\frac{\partial F_B}{\partial t}=f(|E_B|^2,|E_F|^2)E_B\ ,$$

where n_0 and n_1 are given by Eqs. (2.20) and (2.21). The simplest method of handling these equations is to replace the cell with a set of thin slices containing the same number of atoms.[10,27]

Using this procedure, and an input pulse fitted to those of Fig. 10(a), yields the transmitted pulse shapes in Fig. 10(c), in pleasing agreement with the observed pulse shapes [Fig. 10(b)], especially since only measured parameters are used: α is 0.025 cm^{-1} at 10 Torr, and scales as p^2, $I_s \sim 2.3$ MW cm^{-2} at 20 Torr (2.5 MW cm^{-2} at 30 Torr). The value $I/I_s=7$ is thus in line with the measured input intensities in the range 10–20 MW/cm^2.

This good, if somewhat surprising agreement encouraged the development of the numerical code based on that used for Fig. 10(c), but now using finite differences rather than slices. Reservoir effects are incorporated using (3.8), on the reasonable assumption that the reservoir grating is completely washed out. We also account crudely for transverse effects by summing the separate contributions from elemental slices of the transverse intensity distribution of the input signal.

The data for a pressure of 10 Torr is not significantly different to that predicted by plane-wave analysis, Fig. 10(c). In contrast, for high-pressure operation where chaotic emission is observed [Figs. 11(b) and 11(c)], predicted behavior is sensitively dependent on the inclusion of both transverse effects and reservoir features. For comparison we show in Fig. 12 simulated PZT scans for the operating conditions applicable to the high-pressure data of Fig. 11(b), where set (a) is for the simple two-level scheme under plane-wave approximation, set (b) includes transverse effects, and set (c) also accounts for reservoir population transfer (the four-level scheme). The general features of scan (c) are seen to give quite good agreement with our experimental findings. Comparing scans (a) and (b), the significant reductions in the amplitude of oscillation with the inclusion of transverse effects is attributable to different phasing of the oscillation at different radii. Inclusion of reservoir effects [compare traces (b) with (c)] leads to modification of the pulse envelope; to be expected since this manifests the dynamic population distribution in the radiatively coupled transition, which in turn is affected by the finite relaxation time for population transfer from the reservoir levels (the rotational manifolds).

As further corroboration of the instability phenomena predicted for our system and also towards eventual generation of these effects under cw conditions we have extended analysis to the cw regime. We consider the simple two-level scheme with parameter values similar to those for pulsed operation [Fig. 10(b)]. Figure 13(a) shows a coarse cavity tuning scan for fixed cw input intensity of

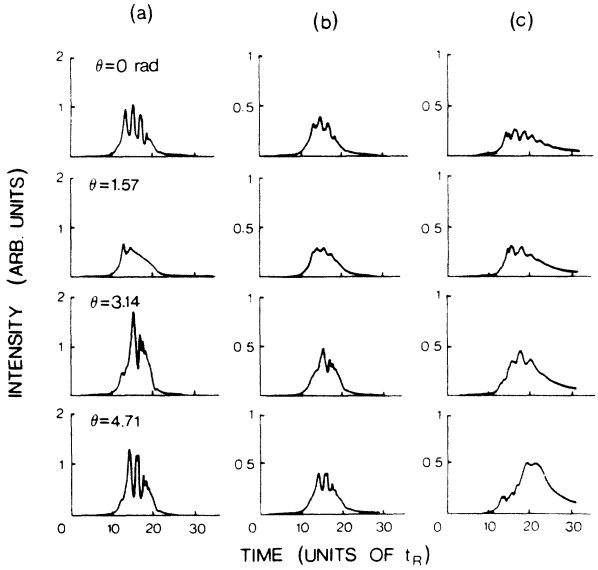

FIG. 12. Predicted transmitted pulse shape at NH_3 pressure 20 Torr for (a) simple two-level scheme, (b) two-level scheme with transverse effects, (c) four-level scheme (reservoir population transfer). [Parameter values as for the experimental values of Fig. 10(b).]

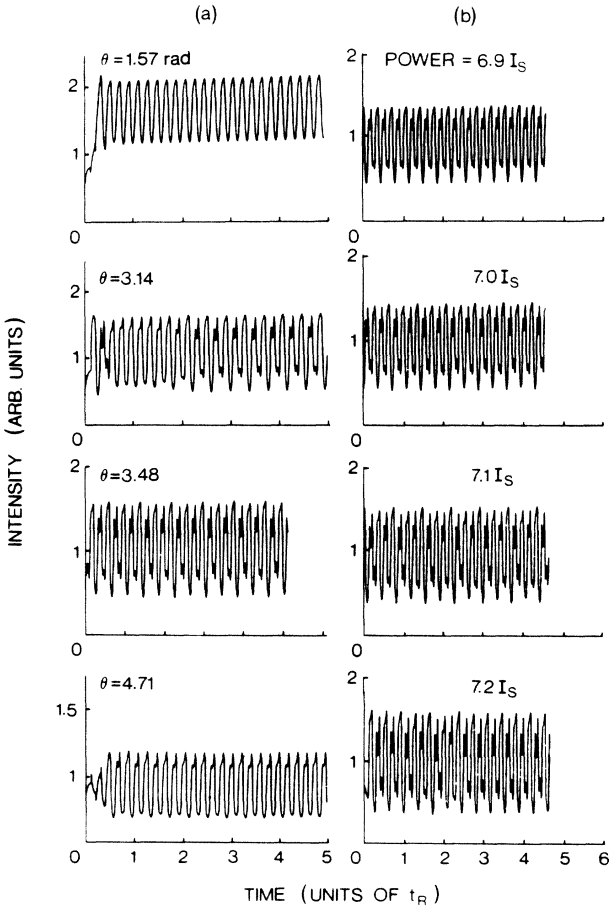

FIG. 13. Predicted cw transmitted pulse shape at NH_3 pressure 20 Torr for simple two-level scheme (a) cavity tuning scan for fixed input intensity of $7I_s$, (b) input intensity scan for fixed cavity tuning ($\theta=3.48$ rad). (Other parameter values as for Fig. 12.)

$7I_s$ as for data of Fig. 11(b). Oscillation initially at period $2t_R$ bifurcates on cavity tuning to $4t_R$ and subsequently $8t_R$ oscillation at an optimum detuning setting of $\theta=3.48$ rad. Further cavity tuning over its free-spectral range results in reversal of the sequence back to $2t_R$ modulation as expected. Evidently the input intensity here is not quite sufficient to drive the cavity signal to a chaotic state. Selecting the detuning for period-eight modulation the input intensity was varied over the small range $6.9I_s$ to $7.2I_s$ [Fig. 13(b)]. Oscillation at period $4t_R$ for an input of $6.9I_s$ bifurcates to period $8t_R$ on increasing to $7I_s$; the original value. For further increase in signal strength to $7.2I_s$ the transmitted signal shows evidence of the onset of chaotic behavior.

The practical realization of these effects under cw conditions is, of course, precluded by the relatively high saturation intensity of this transition requiring input signals of ~ 10 MW/cm^2. Molecules with transitions in closer coincidence with the pump wavelengths and with larger transition moments are clearly favored here. One such molecule considered in preliminary studies is sulfur hexafluoride. Various lines of the $10P$ band of the CO_2 laser were used to excite the dense and broad spectral features of the ν_3 vibrational mode of SF_6. Effects of switching, power limiting, and overshoot, with nanosecond response time have been routinely obtained[28] although generation of instability was precluded in our system since operation was in the bad cavity limit. Significantly, for SF_6, which exhibits both low-saturation intensity and high absorption cross section, switching was readily obtained in cavities with gas cells as thin as 1 mm.

For ammonia we finally note the generality of our results with the observations of bistability and $2t_R$ oscillation using other TEA laser lines again close to resonance and exhibiting self-focusing in ammonia. The PZT scan shown in Fig. 14(a) (for $\frac{1}{2}$ a free-spectral range) exhibiting $2t_R$ modulation was obtained with the $9P(20)$ line at 9.55 μm, pumping the $sR(3,0)$ transition 13.8 GHz above resonance;[29] Fig. 14(b), showing strong pulse distortion, similar to those previously obtained for the $aR(1,1)$ transition, was obtained with the $10R(10)$ line at 10.32 μm possibly pumping the $sQ(1,1)$transition.[22] Oscillation was not obtained for this transition.

V. CONCLUSION

In summary, we have observed optical bistability, period doubling, higher-harmonic oscillations, and chaos in all-optical, ring, and Fabry-Perot resonators containing NH_3 gas as the nonlinear medium. All these effects have been shown to be in qualitative agreement with a simple mathematical model. These results establish the suitability of gases for observations of such phenomena, because of flexibility in the degree of resonant enhancement through choice of transition, of response time through pressure variation, and of linear optical properties (finesse, etc.) through simple independent control of cavity length, cell length, and, again, pressure. The optical systems discussed in this paper are of particular interest because of the possibility of using such systems as a bridge between turbulence and quantum systems. The oscillatory instabilities may lead to the development of passive all-optical modulators,[30] which could find wide application in optoelectronics and laser spectroscopy.

In the experiments reported here we have argued that rotational relaxation is the significant energy-transfer mechanism responsible for the instability phenomena we

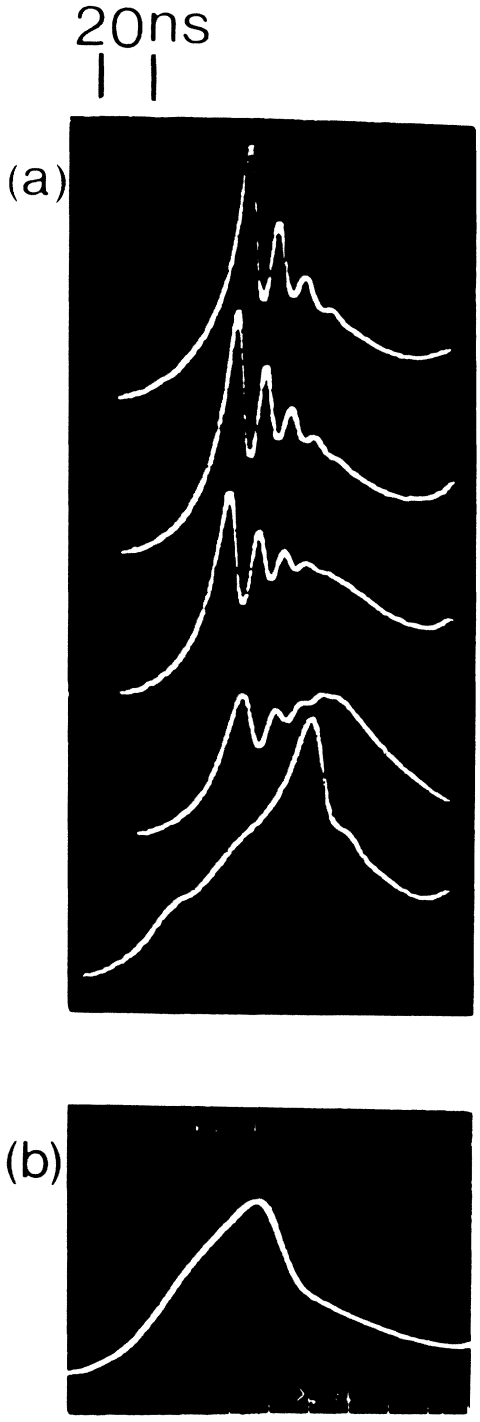

FIG. 14. (a) PZT scan (over $\frac{1}{2}$ free-spectral range) of transmitted signal showing $2t_R$ modulation; NH_3 transition $sR(3,0)$, pressure 22 Torr. (b) Pulse shaping; NH_3 transition $sQ(1,1)$, pressure 30 Torr. Cavity parameters as for Fig. 10.

observe. For our pulsed experiments the considerably slower processes of V-V and V-T relaxation have little effect within the time scale of the input signal. However operation under truly cw conditions will be necessarily controlled by the V-T relaxation rate since this is the limiting process for recycling of population from the rotational-level manifold of the excited vibrational-level state back to ground. Relaxation times τ_v for V-T processes are typically microseconds; for NH_3 $\tau_v \sim 1$ μs Torr, whereas for SF_6, $\tau_v \sim 122$ μs Torr. Saturation intensities associated with this process are therefore advantageously very low (for $SF_6 \sim 6$ W/cm^2),[31] though at the expense of the long medium response time which will normally preclude generation of instability effects. However, a significant virtue of the gas phase is in the use of buffer gas to control response time. This versatility should readily enable optimization of a system for cw conditions.

ACKNOWLEDGMENTS

We gratefully acknowledge the Science and Engineering Research Council for supporting this work. One of us (I.A.Al-S.) acknowledges the Government of Iraq for financial support.

[1] *Optical Bistability 2,* edited by C. M. Bowden, H. M. Gibbs, and S. L. McCall (Plenum, New York, 1983).
[2] L. P. Kadanoff, Phys. Today, **36** (12), 46 (1983); *Chaos and Order in Nature,* edited by H. Haken (Springer-Verlag, Berlin, 1981).
[3] K. Ikeda, H. Daido, and O. Akimoto, Phys. Rev. Lett. **45**, 709 (1980).
[4] K. Ikeda, Opt. Commun. **30**, 257 (1979).
[5] H. M. Gibbs, F. A. Hopf, D. L. Kaplan, and R. L. Shoemaker, Phys. Rev. Lett. **46**, 474 (1981).
[6] H. Nakatsuka, S. Asaka, H. Itoh, K. Ikeda, and M. Matsuoka, Phys. Rev. Lett. **50**, 109 (1983).
[7] A. C. Walker, F. A. P. Tooley, M. E. Prise, J. G. H. Mathew, A. K. Kar, M. R. Taghizadeh, and S. D. Smith, Philos. Trans. R. Soc. London Ser. A **313**, 249 (1984).
[8] F. Shimizu, J. Chem. Phys. **52**, 3572 (1970).
[9] R. G. Harrison, W. J. Firth, C. A. Emshary, and I. A. Al-Saidi, Phys. Rev. Lett. **51**, 562 (1983).
[10] R. G. Harrison, W. J. Firth, and I. A. Al-Saidi, Phys. Rev. Lett. **53**, 258 (1984).
[11] W. J. Firth, Opt. Commun. **39**, 343 (1981); W. J. Firth, E. Abraham, and E. M. Wright, Appl. Phys. B **28**, 170 (1982).
[12] M. J. Feigenbaum, J. Stat. Phys. **19**, 25 (1978).
[13] J. V. Moloney, Phys. Rev. Lett. **53**, 556 (1984).
[14] E. Abraham and W. J. Firth, Opt. Acta **30**, 1541 (1983).
[15] L. A. Lugiato, M. Gronchi, and R. Bonifacio, Opt. Commun. **30**, 129 (1979).
[16] W. J. Firth, E. M. Wright, and E. H. J. Cummins, in *Optical Bistability 2,* edited by C. M. Bowden, H. M. Gibbs, and S. L. McCall (Plenum, New York, 1983), p. 111.
[17] F. A. Hopf, M. W. Derstine, H. M. Gibbs, and M. C. Rushford, in *Optical Bistability 2,* edited by C. M. Bowden, H. M. Gibbs, and S. L. McCall (Plenum, New York, 1983), p. 67.
[18] W. Fuss and K. L. Kompa, Prog. Quantum Electron. **7**, 117 (1981).
[19] C. H. Townes and A. L. Schawlow, *Microwave Spectroscopy* (McGraw-Hill, New York, 1955).
[20] J. L. Lachambre, P. Lavigne, G. Otis, and M. Noel, IEEE J. Quantum Electron. **QE-12**, 756 (1976).
[21] A. Gondhalekar, N. R. Heckenberg, and E. Holzhauer, Phys. Lett. **46A**, 229 (1973).
[22] J. S. Garing, H. H. Nielsen, and K. Narahari Rao, J. Mol. Spectrosc. **3**, 496 (1959); T. Y. Chang, Opt. Eng. **20**, 220 (1981).
[23] I. Burak, P. L. Houston, D. G. Soutton, and J. I. Steinfeld, IEEE J. Quantum Electron. **QE-7**, 73 (1971).
[24] P. K. Gupta and R. G. Harrison, IEEE J. Quantum Electron. **QE-17**, 2238 (1981).
[25] I. A. Al-Saidi, D. Biswas, C. A. Emshary, and R. G. Harrison, Opt. Commun. **52**, 336 (1985).
[26] R. G. Harrison, W. J. Firth, C. A. Emshary, and I. A. Al-Saidi, Appl. Phys. Lett. **44**, 716 (1984).
[27] H. J. Carmichael and J. A. Hermann, Z. Phys. B **38**, 365 (1980).
[28] R. G. Harrison, I. A. Al-Saidi, E. J. Cummins, and W. J. Firth, Appl. Phys. Lett. **46**, 532 (1985).
[29] Y. Noshi, Y. Horiuchi, S. Wada, N. M. Sokabe, and A. Murai, Jpn. J. Appl. Phys. **21**, 719 (1982).
[30] R. G. Harrison, W. J. Firth, I. A. Al-Saidi, and E. Cummins, in *Proceedings of the Topical Meeting on Digital Opical Technology, Schiersee, Germany, 1984,* Advisory Group for Aerospace Research and Development (AGARD) Conference Proceedings No. 362, edited by Billy L. Dove (AGARD, Neuilly Sur Seine, France, 1985), p. 4-1.
[31] H. Brunet, IEEE J. Quantum Electron. **QE-6**, 678 (1970).

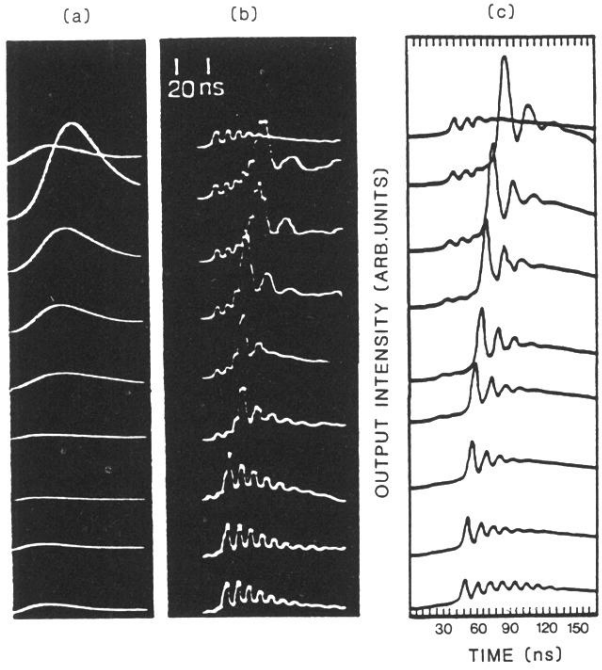

FIG. 10. PZT scan of (a) empty cavity; (b) cavity with 10 Torr NH_3 in 70-cm cell ($L = 86$ cm); input and output reflectivities 67% and 76%, respectively; (c) computer traces for parameters corresponding to (b); $\alpha L = 1.5$, $\Delta \sim 10$; tick spacing t_R.

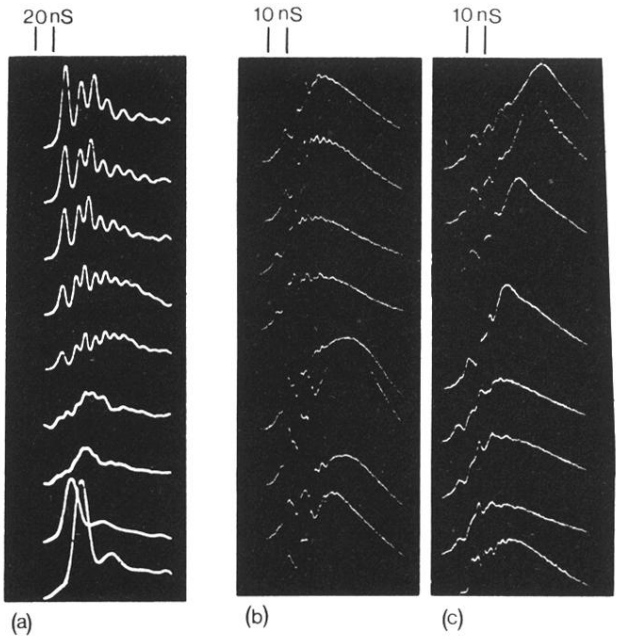

FIG. 11. PZT scan showing (a) $4t_R$ modulation at 5.5 Torr; (b) $2t_R$, $2t_R/3$, and $4t_R/3$ modulation at 19 Torr; and (c) aperiodicity in the modulation at 15 Torr. Cavity parameters as for Fig. 10 but with $R_0 = 36\%$.

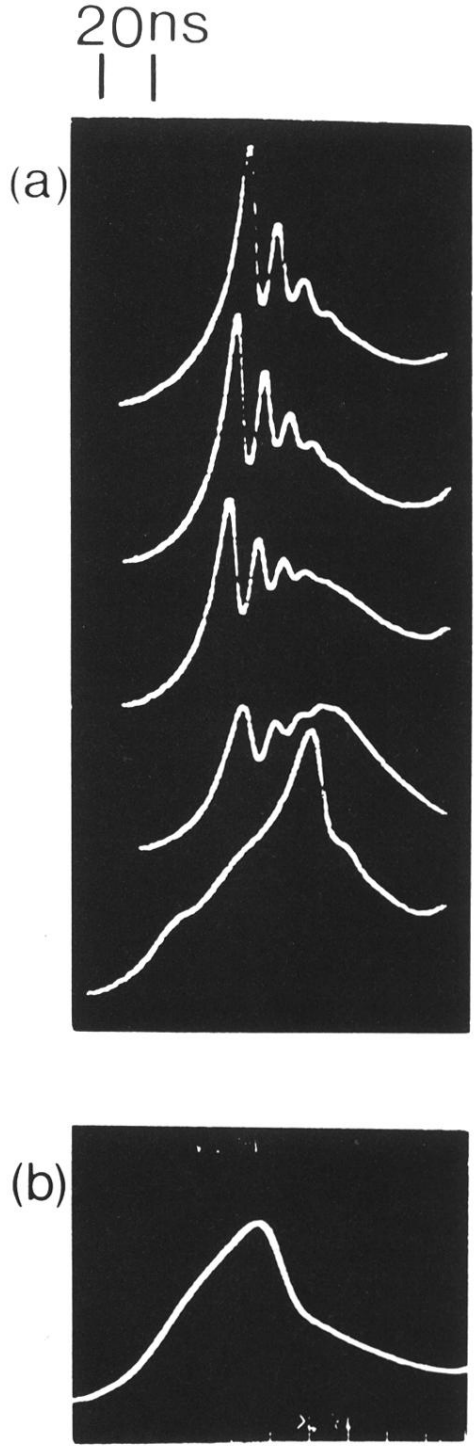

FIG. 14. (a) PZT scan (over $\frac{1}{2}$ free-spectral range) of transmitted signal showing $2t_R$ modulation; NH_3 transition $sR(3,0)$, pressure 22 Torr. (b) Pulse shaping; NH_3 transition $sQ(1,1)$, pressure 30 Torr. Cavity parameters as for Fig. 10.

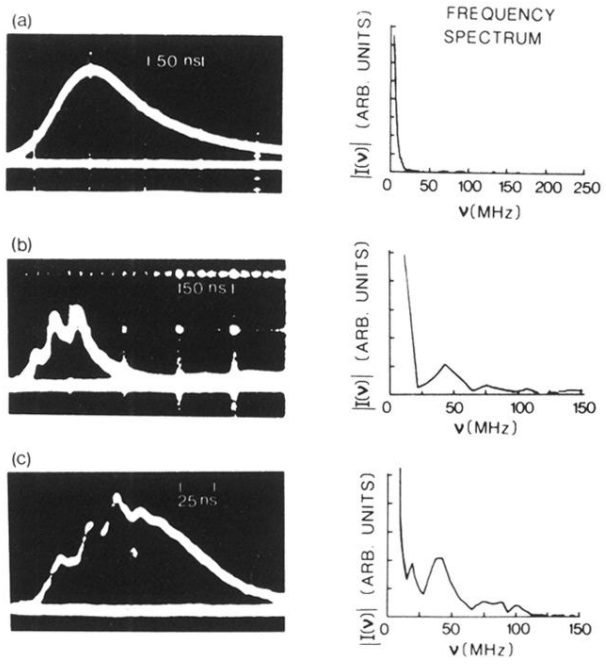

FIG. 7. Sample oscilloscope traces of (a) the pump signal, and (b) and (c) the ring-cavity signal, together with their frequency spectra showing period $2t_R$ in (b) and (c) with indication of $4t_R$ in (c).

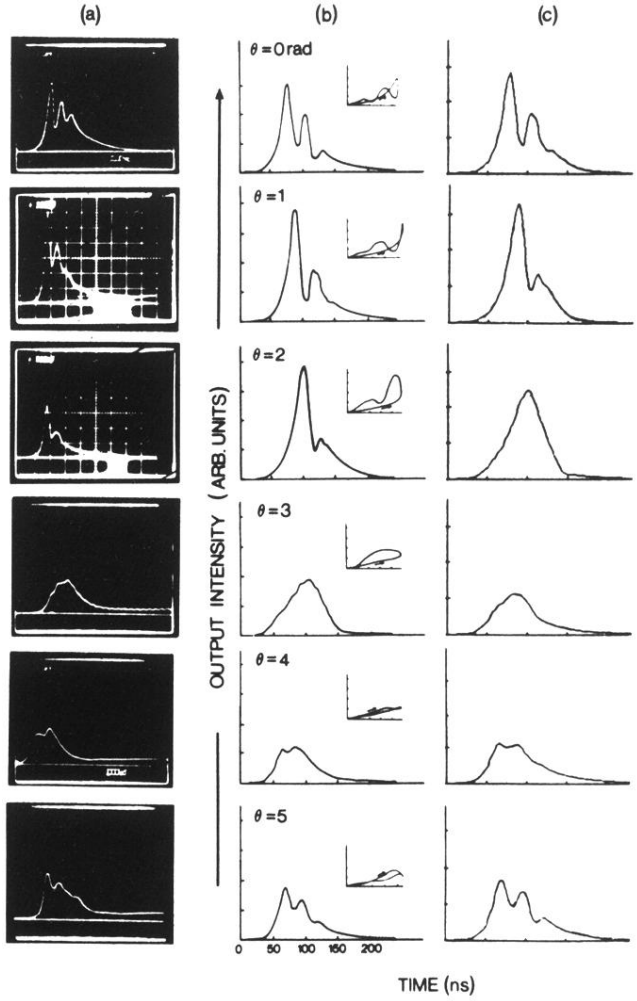

FIG. 8. Sample oscilloscope traces: (a) the ring-cavity signal, together with corresponding theoretical pulse shapes for various detuning angles θ; for (b) the four-level scheme (also showing hysteresis curves of instantaneous cavity signal intensity against incident signal intensity) and (c) the two-level scheme. ($\alpha L = 3$, $kt_R = 5$, $Kt_R = 0.1$, $|\epsilon|^2_{\max} = 0.9$.)